COMPONENT PART NOTICE

THIS PAPER IS A COMPONENT PART OF THE FOLLOWING COMPILATION REPORT:

TITLE: Transonic and Supersonic Phenomean in Turbomachines: Proceedings of the Propulsion and Energetics (68th)(B) Specialists' Meeting Held in Munich, Germany on 10-12 September 1986.

TO ORDER THE COMPLETE COMPILATION REPORT, USE AD-A182 996.

THE COMPONENT PART IS PROVIDED HERE TO ALLOW USERS ACCESS TO INDIVIDUALLY AUTHORED SECTIONS OF PROCEEDING, ANNALS, SYMPOSIA, ETC. HOWEVER, THE COMPONENT SHOULD BE CONSIDERED WITHIN THE CONTEXT OF THE OVERALL COMPILATION REPORT AND NOT AS A STAND-ALONE TECHNICAL REPORT.

THE FOLLOWING COMPONENT PART NUMBERS COMPRISE THE COMPILATION REPORT:

AD#: AD-P005 506 thru AD-P005 523.	AD#:
AD#:	AD#:
AD#:	AD#:

Accession For		
NTIS GRA&I	☑	
DTIC TAB	☐	
Unannounced	☐	
Justification		
By		
Distribution/		
Availability Codes		
Dist	Avail and/or Special	
A-1		

This document has been approved for public release and sale; its distribution is unlimited.

DTIC FORM MAR 85 463

OPI: DTIC-TID

SHOCK STRUCTURE MEASURED IN A TRANSONIC FAN USING LASER ANEMOMETRY

Jerry R. Wood and Anthony J. Strazisar
National Aeronautics and Space Administration
Lewis Research Center
Cleveland, Ohio 44135, USA
and
P. Susan Simonyi
Sverdrup Technology, Inc.
Middleburg Heights, Ohio 44130, USA

SUMMARY

Shock structure measurements acquired in a low aspect ratio transonic fan rotor are presented and analyzed. The rotor aspect ratio is 1.56 and the design tip relative Mach number is 1.38. The rotor flowfield was surveyed at near maximum efficiency and near stall operating conditions. Intra-blade velocity measurements acquired with a laser fringe anemometer on blade-to-blade planes in the supersonic region from 10 to 60 percent span are presented. The three-dimensional shock surface determined from the velocity measurements is used to determine the shock surface normal Mach number in order to properly calculate the ideal shock jump conditions. The ideal jump conditions are calculated based upon the Mach numbers measured on a surface of revolution and based upon the normal Mach number to indicate the importance of accounting for shock three dimensionality in turbomachinery design. Comparison of the shock locations with those predicted by a 3D Euler code showed very good agreement and indicated the usefulness of integrating computational and experimental work to enhance understanding of the flow physics occurring in transonic turbomachinery passages.

INTRODUCTION

Advanced fans and core compressor inlet stages feature low aspect ratio, highly loaded rotors which operate in the transonic regime. Much of the total pressure rise which occurs in these rotors is due to the rotor passage shock. Accurate models of the passage shock are therefore required for use in the blade design process.

Until recent years, the classic Miller-Lewis-Hartman shock model has been used in many blade design systems. This model is based on the assumption that the shock surface is normal to u blade-to-blade streamsurface and is oriented normal to the suction surface of the rotor blade. Prince [1] and Wennerstrom [2] have attempted to refine this model to include the effects of shock obliquity in both the blade-to-blade and spanwise direction. The refined models are based on analysis of high-response rotor tip static pressure measurements and empirical arguments.

As part of a NASA Lewis Research Center program aimed at obtaining detailed flowfield measurements within turbomachinery blade rows, a transonic axial fan rotor has been extensively surveyed using laser anemometry. Results from this effort include detailed velocity surveys through the rotor passage shock system. An analysis of this data is the subject of this report. The shock surface shape and orientation are presented for the near stall and peak efficiency operating conditions. Several qualitative features of the rotor passage shock are found to be in agreement with empirical arguments set forth by Prince [1]. The shock jump conditions are calculated for the three dimensional shock and are compared to those obtained when spanwise obliquity of the shock is neglected. The results indicate that spanwise obliquity of the shock must be taken into account in order to obtain accurate predictions of the shock strength. The results are also consistent with the laser anemometer measurements which indicate that the shock strength is weaker than one would expect if one assumes that the shock surface is normal to a blade-to-blade streamsurface. The shock locations on the suction surface are compared to isomach lines obtained from a numerical calculation of the three dimensional Euler equations coupled with a two dimensional boundary layer code. The agreement in terms of spanwise lean is excellent.

COMPRESSOR ROTOR

The test vehicle for the present study is a low aspect ratio fan rotor. The rotor design pressure ratio is 1.63 at a mass flow of 33.25 kg/s. The tip relative Mach number is 1.38 at the design tip speed of 429 m/s. The rotor has 22 blades, an aspect ratio of 1.56 (based on average span/root axial chord), an inlet tip diameter of 51.3 cm, and an inlet hub/tip radius ratio of 0.375. The rotor tip clearance at design speed is 0.5 mm. The rotor does not have a part-span shroud which is typically found in fan rotors of higher aspect ratio. Details of the rotor aerodynamic design are given in [3].

The results reported herein where obtained in a rotor-only configuration with no inlet guide vane or stator installed. The rotor-only design speed operating line is shown in Figure 1. Massflow rate is measured across a calibrated orifice located far upstream of the fan rotor. The rotor total pressure rise and efficiency are measured using conventional pressure and temperature survey instrumentation.

INSTRUMENTATION

The laser fringe anemometer (LFA) system used in the present investigation is a single-channel, dual-beam system with an on-axis backscatter light collection scheme and has previously been described in detail in [4] and [5]. Access to the compressor flowfield is through a 3 mm thick glass window. The window curvature conforms to the rotor outer flowpath, thereby minimizing disturbances to the tip region flow. Fluorescent seed particles with a nominal diameter of 1-1.4 microns are spray atomized and injected into the flow stream through a 6mm diameter tube located 60 cm upstream of the rotor leading edge. Data from the conventional pressure and temperature survey instrumentation is used to control the on-line operating condition set point.

The LFA measurement locations in the meridional plane and in the blade-to-blade plane at 10 percent span are shown in Figure 2. Conventional pressure and temperature data are obtained at stations 1 and 2 in the figure. LFA measurements are acquired along conical measurement surfaces which pass through radii corresponding to 10 percent mass flow fractions at the rotor trailing edge. These conical surfaces are generated by straight-line interpolation between design streamline radii which are known at stations 1 and 2 and at the blade edges. Measurement locations are distributed axially at 20 percent chord intervals from -100 percent to -20 percent chord, at -10 percent chord, and at 2.5 percent chord intervals from -5 percent chord to 10 percent chord. For the near stall operating condition, measurement locations are distributed at 10 percent chord intervals from 10 percent chord to the rotor trailing edge. For the peak efficiency operating condition, the measurement locations are distributed at 2.5 percent chord intervals from 10 percent chord to the rotor trailing edge. The increased axial density of measurement locations used at peak efficiency is required in order to resolve two-shock systems which occur within the rotor at backpressure levels at and below the peak efficiency operating point.

The circumferential location of each LFA velocity measurement relative to the rotor is determined by assigning the measurement to a "window" formed by adjacent pulses generated by a variable frequency clock that is phase-locked to the rotor rotational speed. All measurements that occur within a measurement window are averaged together and assigned to the center of the window. The clock frequency is set to generate 50 measurement windows across a blade pitch. LFA measurements are acquired across 17 of the 22 rotor blade passages. A typical data collection run consists of collecting 60,000 velocity measurements at each axial survey location. This yields approximately 70 measurements in each individual measurement window and results in a circumferential velocity profile in each of 17 individual blade passages. These 17 profiles are spatially averaged together to form an "average" blade passage velocity profile. The mean velocity calculated in each of the 50 measurement windows in this "average" profile is therefore based on approximately 1200 measurements.

Velocity magnitude and flow angle are determined using measurements acquired at two different angular orientations of the fringe system at each axial survey location. Just prior to performing a complete flowfield survey, screening runs are made to determine the axial distribution of the pitchwise-averaged flow angle along the measurement streamsurface. The fringe orientations which are used at each axial survey location are then chosen so as to bracket the local pitchwise-averaged absolute flow angle by 20 degrees.

SEED PARTICLE LAG EFFECTS

The velocity measured immediately downstream of a shock is known to be higher than the true gas velocity because the seed particles have finite inertia and cannot follow the high deceleration rates across a shock. This phenomena is known as seed particle lag. The extent of the region in which seed particle lag effects are present and the magnitude of the lag are functions of the seed particle size and the shock strength. The particle size and shock strength parameters in the present work are nearly identical in value to those of an earlier investigation [4], in which seed particle lag effects were studied. Results from [4] indicate that for a normal shock at an upstream Mach number of 1.4 the velocity measured behind the shock lags behind the true velocity for a streamwise distance of 12 mm, which corresponds to 12 percent of aerodynamic chord for the present rotor. Within this lag region, the measured velocity is given approximately by

$$V_p = V_{g1} + (V_{g1} - V_{g2}) * \exp(-3\, X/L) \qquad (1)$$

where V_p is the measured seed particle velocity, V_{g1} and V_{g2} are the true gas velocities upstream and downstream of the shock, respectively, X is the streamwise distance downstream of the shock, and L is the lag distance.

Schodl [6] has investigated the effects of particle size on the Mach number distribution measured across a shock by comparing measurements acquired with a laser transit anemometer across an axial compressor rotor bow shock for a range of particle sizes. He found that although the post-shock Mach number distribution is dependent on particle size, the point at which the Mach number first begins to change rapidly is independent of particle size. Therefore, when determining the shock location in the present study, the point at which the measured Mach number first begins to change is considered to be an accurate and consistent indicator of the shock location.

DETERMINATION OF SHOCK SURFACE LOCATION

The shock location is determined on each measurement surface between 10 and 60 percent span by inspecting blade-to-blade distributions of relative Mach number at each axial measurement point as well as streamwise distributions of Mach number at constant pitch relative to the blade suction surface. Typical blade-to-blade and streamwise Mach number distributions are shown in Figure 3, along with the shock location. The measurements shown in this figure were acquired on the 30 percent span measurement surface for the peak efficiency operating condition. Both the blade-to-blade and streamwise Mach number distributions indicate the existence of a two-shock system within the rotor. The second shock occurs only at back pressure levels at or below the peak efficiency operating point and rarely shows up as clearly in blade-to-blade plots as it does in Figure 3. Streamwise plots of relative Mach number are found to provide a much more sensitive indication of the second shock location. In order to improve the spatial resolution of the streamwise Mach number distributions, LFA surveys are taken every 2.5 percent of rotor chord at the peak efficiency operating condition.

The locus of shock location data points determined using the above procedure is shown for the peak efficiency and near stall operating conditions in Figures 4 and 5, respectively. The shock is shown extending from the suction surface to its intersection near the blade leading edge with a line extrapolated from the blade mean camber line. Only the front shock is shown at each span for the peak efficiency condition. At the near stall flow there appeared to be a weak front lambda shock near the blade suction surface followed by a stronger rear leg. The shock plots for near stall reflect only the rear portion of the lambda which produced the majority of the flow deceleration. The uncertainty in the shock location is on the order of two measurement windows (4 percent of rotor pitch) in the circumferential direction and one percent of rotor chord in the streamwise direction. The solid curve in each figure is determined by a least-squares polynomial curve fit of the shock location data points. This curve fit is performed in order to obtain an analytically smooth description of the shock in the blade-to-blade streamsurface. Eleven points along the shock face are determined from the fitted curve for use in plotting the three-dimensional shock surface shape and in performing calculations of the shock jump conditions.

The shock shapes at 10 percent through 40 per cent span are consistent with the model proposed by Prince [1] in that they are approximately axial over most of the passage width before turning to normal at the suction surface. At 10, 20 and 30 percent spans the intersection of the axial and normal portions of the shock occurs at approximately 75, 76 and 83 percent passage width, respectively. This compares quite well to Prince's estimate of 85 percent passage width. Shock stand-off distance at these spans are approximately 2.5 percent chord. At 40, 50 and 60 percent spans, the stand-off distances are approximately 6.6, 8.9 and 8.4 percent of chord, respectively. The estimated error in determining stand-off distance is about 1.7 percent of chord.

CALCULATION OF JUMP CONDITIONS ACROSS THE SHOCK

In order to calculate the jump conditions across the shock which satisfy the relations for conservation of mass, normal momentum, tangential momentum, and energy together with the requirement that the entropy does not decrease, it is necessary to determine the normal vector to the three dimensional shock surface in the rotor passage. The normal is calculated by assuming that the shock surface can be described by some function

$$G(\theta,R,Z) = 0 = \theta - F(R,Z) \qquad (2)$$

where θ, R, Z are the axes for a cylindrical coordinate system. Consequently,

$$\theta = F(R,Z) \qquad (3)$$

The normal vector, $\hat{n}$, can be obtained by

$$\hat{n} = \frac{\nabla G}{\left[\nabla G \cdot \nabla G\right]^{1/2}} = \frac{\hat{e}_\theta - R\frac{\partial\theta}{\partial R}\hat{e}_R - R\frac{\partial\theta}{\partial Z}\hat{e}_Z}{\left[1 + \left(R\frac{\partial\theta}{\partial R}\right)^2 + \left(R\frac{\partial\theta}{\partial Z}\right)^2\right]^{1/2}} \qquad (4)$$

where $\hat{e}_\theta$, $\hat{e}_R$, and $\hat{e}_Z$ are the unit vectors in the cylindrical coordinate system. The partial derivatives are obtained using numerical differentiation.

The shock face Mach numbers were obtained from the velocity components measured in the θ,Z plane and assuming the radial velocity ahead of the shock could be calculated from the measured axial component of velocity and the design streamline slopes for the rotor. The maximum design streamline slope was -8.3 degrees at 10 percent span from the tip which did not significantly change the Mach number. The Mach number component normal to the surface is obtained from

$$M_N = \vec{M} \cdot \hat{n} \qquad (5)$$

where the Mach vector, $\vec{M}$, has the same direction as the velocity vector and the same magnitude as the Mach number. The component of the Mach vector tangent to the shock is obtained from

$$\vec{M}_T = \vec{M} - M_N\hat{n} \qquad (6)$$

With the speed of sound before the shock, the velocity component tangent to the shock surface can be obtained. With the normal and tangential components known before the shock, the conservation laws can be applied to yield the after shock conditions.

In order to demonstrate the importance of considering the three dimensional nature of the shock, the after shock conditions were also calculated with the shock assumed to be perpendicular to the conical surface of revolution on which the measurements were taken. The "perceived" normal Mach number which would be obtained if only the two dimensional nature of the shock were considered was calculated in a manner similar to that used to calculate the true normal Mach number. The normal velocity calculated after the shock using the normal Mach number and the normal velocity after the shock using the "perceived", or two dimensional, normal Mach number were used to calculate the Mach number and total conditions after the shock for each case. Although in the frame of reference of the rotor the total temperature across the shock is constant, the total temperature across the shock in the laboratory, or absolute, frame of reference is not constant. A significant increase in total pressure and total temperature occurs across the shock along with a corresponding increase in entropy. The total pressure ratio and the associated isentropic efficiency of the compression across the shock was calculated to demonstrate the difference in calculated rotor work done by assuming a two dimensional shock when the actual shock is three dimensional. The isentropic efficiency, η , was calculated from

$$\eta = \frac{(PR)^{\frac{\gamma-1}{\gamma}} - 1}{TR - 1} \qquad (7)$$

where PR is the total pressure ratio and TR is the total temperature ratio across the shock in the absolute frame of reference and γ is the specific heat ratio.

QUALITATIVE DESCRIPTION OF THE SHOCK SURFACE

Two earlier investigations have attempted to visualize the three dimensional shock surface. This goal is quite difficult to achieve due to the three-dimensional nature of both the rotor blade and the shock itself. In [7] holograms were acquired from a transonic axial fan rotor. A three-dimensional image of the shock surface and blade passage was obtained by reconstructing the hologram within two blades held in a fixture in the laboratory. A pointer was then placed on the shock surface by using parallax while viewing the hologram and blade pair. The pointer locations were then used to place a piece of plastic film within the blade passage at the shock surface location. Photographs of the blade pair with the plastic film attached are included in [7]. In an earlier investigation of the present data [8], plots of the shock locations determined at each span were "stacked" together to obtain a quasi-three dimensional view of the shock surface. This view represented the shock as seen from a single perspective.

In the present work, three dimensional graphics is used to qualitatively study the shock surface shape. The eleven points determined from curve fits of the shock location data in each of the six blade-to-blade measurement surfaces are combined to form an eleven-by-six grid which describes the shock surface shape. This grid is combined with coordinates of the blade suction and pressure surfaces to form a composite graphics image in which the shock appears in the proper orientation relative to the blade. By using surface shading and hidden line techniques as well as coordinate rotation about three orthogonal axes, the shock surface can be studied on a graphics workstation from several different viewing angles. Selected views of the near stall and peak efficiency shock surfaces are shown in Figures 6 and 7, respectively.

Since surface shading could not be illustrated in a black and white format, a mesh plot of figures 6 and 7 was chosen for this report. Although Mach number contours are not visible on the mesh plots the three dimensional characteristics of the shock surface can be shown. The figures illustrate such qualitative features of the shock as spanwise lean, standoff distance of the shock surface from the blade's leading edge, and the overall structure of the shock surface. A comparison of the shock structure between the two operating conditions can easily be made by viewing figures 6 and 7. Three dimensional graphics has proven to be a powerful method of studying the shock surface shape. The technique, however, is most effective when one views the three dimensional image on a graphics workstation.

RESULTS FOR THE JUMP CALCULATIONS ACROSS THE SHOCK

The calculations for the jump conditions across the shock were done only for the shock loci presented and did not attempt to consider the change through a multiple shock system. The results for the near stall flow rate are presented in figures 8 through 10 and show the calculations for the jump conditions across the shock when the actual three dimensional nature of the shock is considered and when the shock is considered to be two dimensional i.e. the shock is perpendicular to the conical surface of revolution. The calculation of the post-shock Mach number for 10, 30 and 50 percent span from the tip is shown in figure 8. The three dimensional nature of the shock is most evident for 50 percent span where the 3D calculations yields an after shock Mach number which is generally 0.20 to 0.26 higher than the 2D calculation. At thirty percent span the difference is between 0.15 and 0.17. At ten percent span the shock is two dimensional except for a slight three dimensional effect near the leading edge which is due to the lean of the leading edge in the streamwise direction. The total pressure rise calculated across the shock in the laboratory frame of reference is shown in figure 9. A large pressure rise occurs across the bow shock for each percent span with the tip shock producing a calculated pressure ratio of 1.57 and the 50 percent span location producing a pressure ratio 1.06. The two dimensional calculation consistently produces more indicated pressure ratio than does the three dimensional calculation. The isentropic efficiency of the compression process across the shock is shown in figure 10. The isentropic efficiency calculated for the two dimensional shock is lower than that calculated for the 3D shock which is consistent with the pressure rise calculated with each method.

Results calculated for the peak efficiency flow point are shown in figure 11 for the calculated Mach number change only since the calculated pressure rise and efficiency followed the same trends as those observed for the near stall flow rate. For 10 percent span the shock is essentially two dimensional up to about 50 percent of the distance along the face of the shock from the leading edge to the suction surface with three dimensional effects occurring over the last 50 percent of the passage. Whereas the two dimensional calculations indicate after shock Mach numbers appreciably less than sonic, the three dimensional calculation indicates after shock Mach numbers that are generally greater than sonic. There is considerably less three dimensional effect at 20 percent span and comparable three dimensional effects at 30 percent and 50 percent spans. The location of the shock foot at peak efficiency is very sensitive to small changes in flow and the large difference in the three dimensional effects at 10 percent and 20 percent may be due in part to difficulty in establishing identical operating conditions for all the percent span locations which were measured on different days.

The three dimensionality of the shock has considerable effect on the assumption that the flow can be treated as streamsurfaces for analysis with either two dimensional or quasi-three dimensional computer codes. At 30 percent span near the leading edge, the flow into the shock is inclined at about -2.0 degrees to the axial direction. After the shock the calculated flow has an inclination of about +9.8 degrees to the axial direction. This also has ramifications on the measured velocities behind the shock since the measurements are taken on the design streamsurface of revolution. Obviously, some of the particles measured downstream of the shock crossed the shock at a different spanwise location than that at which they are being measured after the shock.

Chordwise plots of relative Mach number are shown in Figure 12a for the near stall flow rate for the midpitch position for 10, 30 and 50 percent spans and in Figure 12b for the peak efficiency flow at 20, 50 and 80 percent pitch for 10 percent span. Also shown are the results from the jump calculations across the shock. For the near stall flow at the 10 percent span location the shock is two dimensional and both the 3D and 2D calculations yield an after shock Mach number of about 0.85 at 22 percent chord compared to a measured value of about 0.94 at 40 percent chord. If particle lag is considered then the particles should have reached terminal velocity at about 34 percent chord. Since no detailed data were taken in the 30-40 percent chord range its not possible to determine where the particle deceleration ceased; however, it would appear that they would have attained an after shouk velocity corresponding to about Mach 0.95 to 1.0 at the 34 percent chord location. At 30 percent span the shock is three dimensional with the 3D calculation yielding an after shock Mach number of 0.94 and the 2D calculation yielding a value of 0.79. The experimental data shows an after shock Mach number of about 0.97 at 12 percent chord downstream of the shock. At 50 percent span the shock is also three dimensional with the 3D calculation yielding 1.04 and the 2D calculation yielding 0.84 Mach number. At 12 percent chord downstream of the shock the Mach number from the data appears to be about 0.94. Inspection of the deceleration of the flow from 20 percent to 60 percent chord indicates the passage is increasing in area so that part of the difference between the 3D calculation and the estimated value at 18 percent chord may be due to an increase in flow area in the streamwise direction from the location of the shock to the passage exit.

In [9] the LFA data for this rotor were compared to the results obtained with the 3D Euler computer code described in [10]. Comparisons of the calculations with the experimental data indicated that from 10 to 70 percent span the code gave results which described quite well the locations of the shocks when compared to near-surface Mach numbers in the blade-to-blade plane. Figure (13) shows the projection of the suction surface of the blade onto a meridional plane with the shock locations from the present data and the isomach lines determined from the calculations. In addition to the original views given in [10] for the peak efficiency and near stall flow, an additional result from the code is included for a flow rate slightly smaller than the peak efficiency flow. Peak efficiency flow rate from the experiment was 98.9 percent of the maximum flow rate measured for the rotor. The calculation previously presented for peak efficiency was for a flow rate of 99.2 percent of the maximum flow rate predicted by the computer code for the rotor. In [10] the difference in maximum predicted flow and maximum experimental flow was quoted as 0.06 percent. It was also stated that calculations were made at 98.4 percent flow and 99.8 percent flow and that significantly different locations were predicted for the shock at 10 percent span. The results for the calculations at 98.4 percent flow are also shown on the figure and compared to the measured shock locations. For both flows the three dimensional nature of the shock along the suction surface is well predicted with the best fit being for a flow rate between 98.4 and 99.2 percent of maximum flow. Comparison of the calculated isomach lines and the measured shock locations are also shown for the near stall point. The predicted three dimensional nature of the shock agrees well with the data

Figure (14) shows the results obtained from the code in the blade-to-blade plane for 10 percent span. As stated in [9] the shock location calculated on the suction surface for 98.4 percent flow moved about 15 percent chord from that calculated at 99.2 percent flow. Figure (14) shows the transition of the flow from a two shock system to a single shock in going from 99.2 to 98.4 percent flow. This type of shock structure more nearly matches the model proposed by Wennerstrom [2] than that proposed by Prince [1]. This large movement of the shock at the near peak efficiency flow point for a small change in flow rate (0.8 percent or 0.28 kg/sec) requires matching experimental and computational flow rates very accurately in order to make valid comparisons. It also emphasizes the difficulty of mapping this rotor at many spanwise stations for a flow rate near peak efficiency.

CONCLUDING REMARKS

The present paper has defined the shock structure inside the rotating passage of a low aspect ratio transonic fan at a flow rate near peak efficiency and near stall using detailed data obtained with a laser fringe anemometer. Because of the severe distortion of the shock surface at the peak efficiency flow, it is quite beneficial to qualitativley study the shock structure using three dimensional graphics in an interactive mode. It was also shown that once the shock surface is defined, the normal shock jump conditions can be used to calculate after shock Mach numbers. When particle lag across the shock is considered, the agreement with data was shown to be good. At the near stall flow where the density of the LFA measurements was not as high as that used for the peak efficiency flow, the agreement was not quite as good between the jump calculations and the after shock Mach numbers. Overall the jump calculations indicate the importance of including the three dimensional nature of the shock in interpreting the experimental data. It also emphasizes the need to account for the three dimensionality of the shock as proposed by Prince [1] and Wennerstrom [2] in the design of turbomachinery passages. The total pressure ratio calculated across the shock indicated that a significant portion of the rotor total pressure rise is produced by the shock and that the efficiency of this compression process is quite high.

Comparison of the shock locations with those predicted by a 3D Euler code showed very good agreement and indicated the usefulness of integrating computaional and experimental work to enhance understanding of the flow physics occurring in transonic turbomachinery passages.

References

1. Prince, D.C. Jr., "Three-Dimensional Shock Structure For Transonic/Supersonic Compressor Rotors," AIAA Journal of Aircraft, Vol. 17, No. 1, Jan. 1980, pp. 28-37.

2. Wennerstrom, A.J. and Putterbaugh, S.L., "A Three-Dimensional Model for the Prediction of Shock Losses in Compressor Blade Rows," ASME Paper No. 83-GT-216, 1983.

3. Urasek, D.C., Gorrell, W.T. and Cunnan, W.S., "Performance of a Two-Stage Fan Having Low Aspect Ratio First-Stage Rotor Blading," NASA TP-1493 and AVRADCOM TR 78-49, Aug. 1979.

4. Powell, J.A., Strazisar, A.J. and Seasholtz, R.G., "Efficient Laser Anemometer for Intra-Rotor Flow Mapping in Turbomachinery,' ASME Journal of Engineering for Power, Vol. 103, No. 2, Apr. 1981, pp. 424-429.

5. Strazisar, A.J. and Powell, J.A., "Laser Anemometer Measurements in a Transonic Axial Flow Compressor Rotor," ASME Journal of Engineering for Power, Vol. 103, No. 2, Apr. 1981, pp. 430-437.

6. Schodl, R.G., "A Laser-Two-Focus (L2F) Velocimeter for Automatic Flow Vector Measurements in the Rotating Components of Turbomachines", ASME Journal of Fluids Engineering, Vol. 102, Dec. 1980, pp. 412-419.

7. Wuerker, R. F.; Kobayashi, R. J.; Heflinger, L. O.; and Ware, T.C., "Application of Holography to Flow Visualization Within Rotating Compressor Blade Row, NASA CR-121264, Feb. 1974.

8. Strazisar, A.J.,"Investigation of Flow Phenomena in a Transonic Fan Rotor Using Laser Anemometry," ASME Journal of Engineering for Gas Turbines and Power, Vol. 107, No. 2, Apr. 1985, pp. 427-435.

9. Pierzga, M. J. and Wood, J. R.; "Investigation of the Three-Dimensional Flow Field Within a Transonic Fan Rotor: Experiment and Analysis", ASME Journal of Engineering for Gas Turbines and Power, Vol. 107, No. 2, Apr. 1985, pp. 436-449.

10. Denton, J. D., "An Improved Time Marching Method for Turbomachinery Calculations," ASME Paper 82-GT-239, 1982.

DISCUSSION

J. Chauvin

(1) Do the measurements give information about unsteadiness of the flow, especially about the shock foot motion at the suction surface? Have you information on the flow turbulence?

(2) How close to the stall line was the near stall point?

Author's Reply

In general only the components of velocity and the standard deviation of the velocity histogram were stored because of memory limitations in the dedicated computer. Some data were taken and individual measurements for each window were stored so individual histograms could be studied. Some of this data was discussed by Strazisar [8] and did demonstate movement of the shock at the 20 percent chord location for 10 percent span at the near stall flow. More data was taken in this "data capture mode" but was not taken in sufficient detail to allow study of the shock foot movement. Increased memory capacity on our dedicated computer at NASA Lewis will allow us to do more detailed mappings in order to study shock unsteadiness in the future.

The near stall flow rate was 92.6 percent of the maximum measured flow for the rotor. Unstable operation of the rotor occurred at 91.6 percent of maximum measured flow rate.

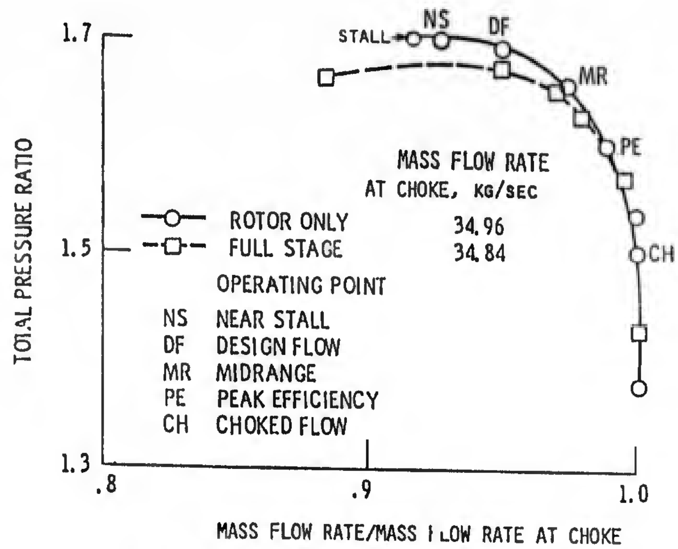

Figure 1.- Rotor design speed operating line.

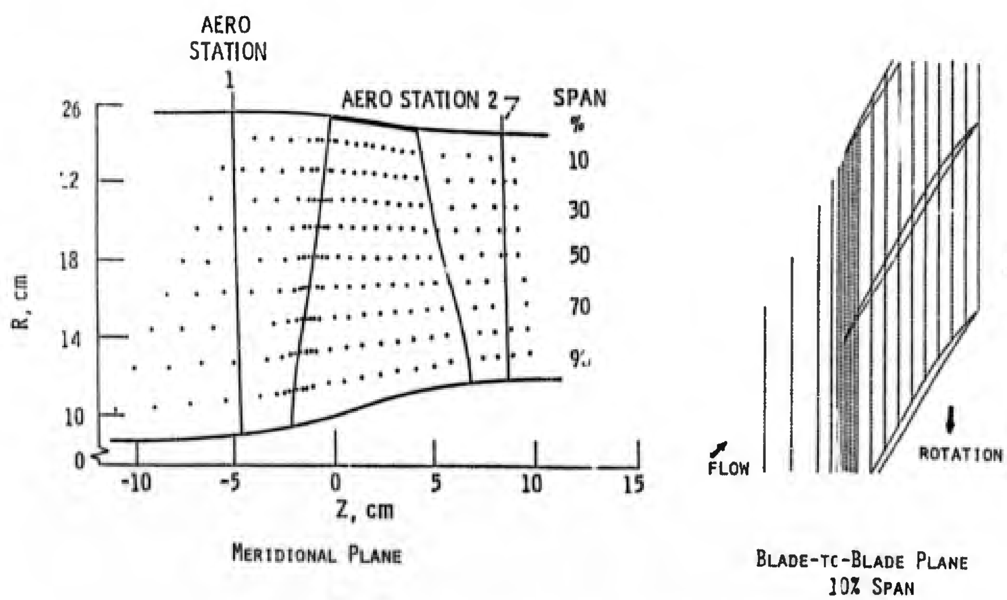

FIGURE 2. - TYPICAL LASER FRINGE ANEMOMETER MEASUREMENT POINTS AND AERODYNAMIC SURVEY LOCATIONS

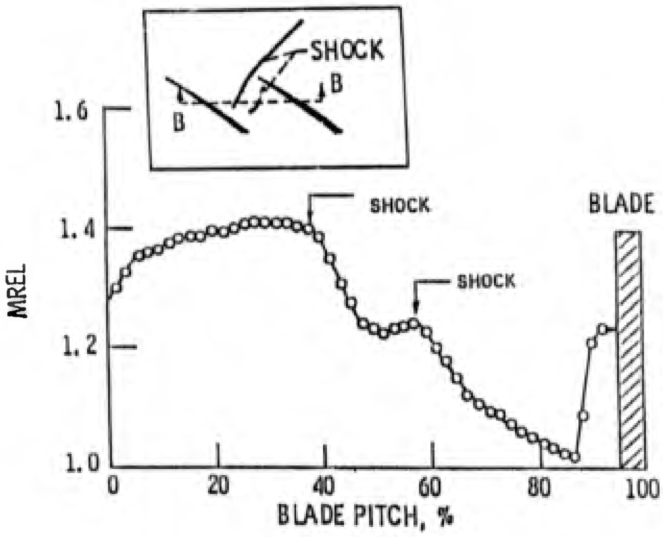

FIGURE 3A. - Blade-to-blade distribution (view B-B of relative Mach number at 30% span, 30% chord at peak efficiency.

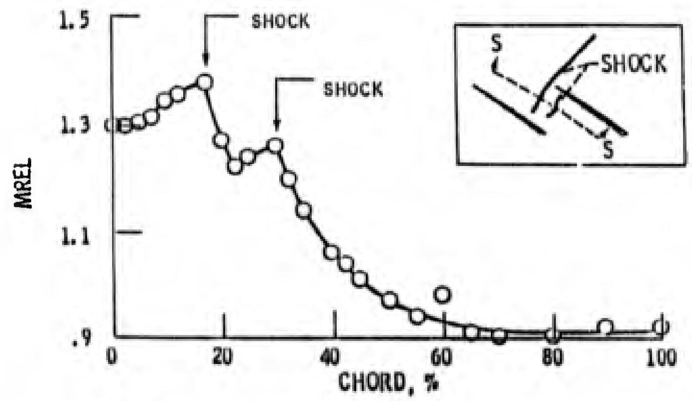

FIGURE 3B. - Streamwise distribution (view S-S) of relative Mach number at 30% span, 60% blade pitch from the suction surface at peak efficiency.

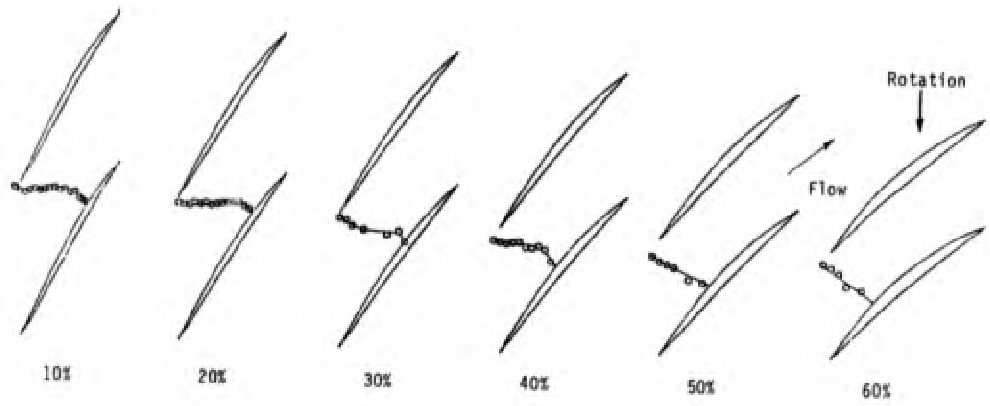

Figure 4. - Shock location in blade-to-blade plane for six spanwise locations at Near Stall Flow Rate.

o - Shock Location
— - Curvefit of Data

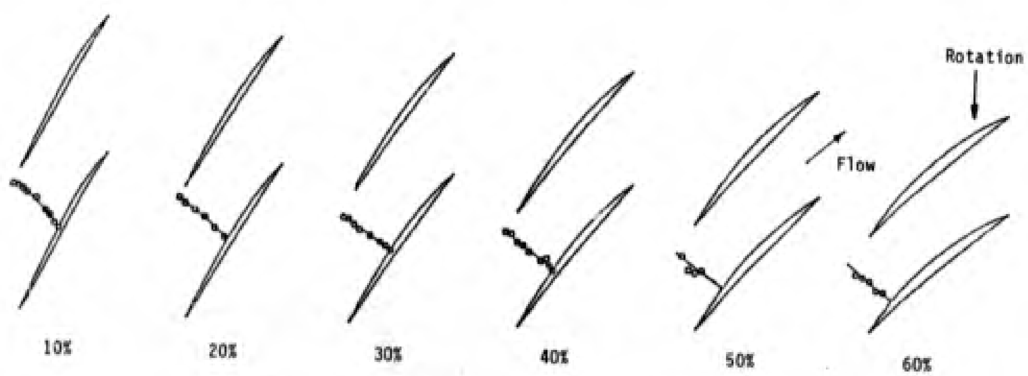

Figure 5. - Shock location in blade-to-blade plane for six spanwise locations at Peak Efficiency Flow Rate.

o - Shock Location
— - Curvefit of Data

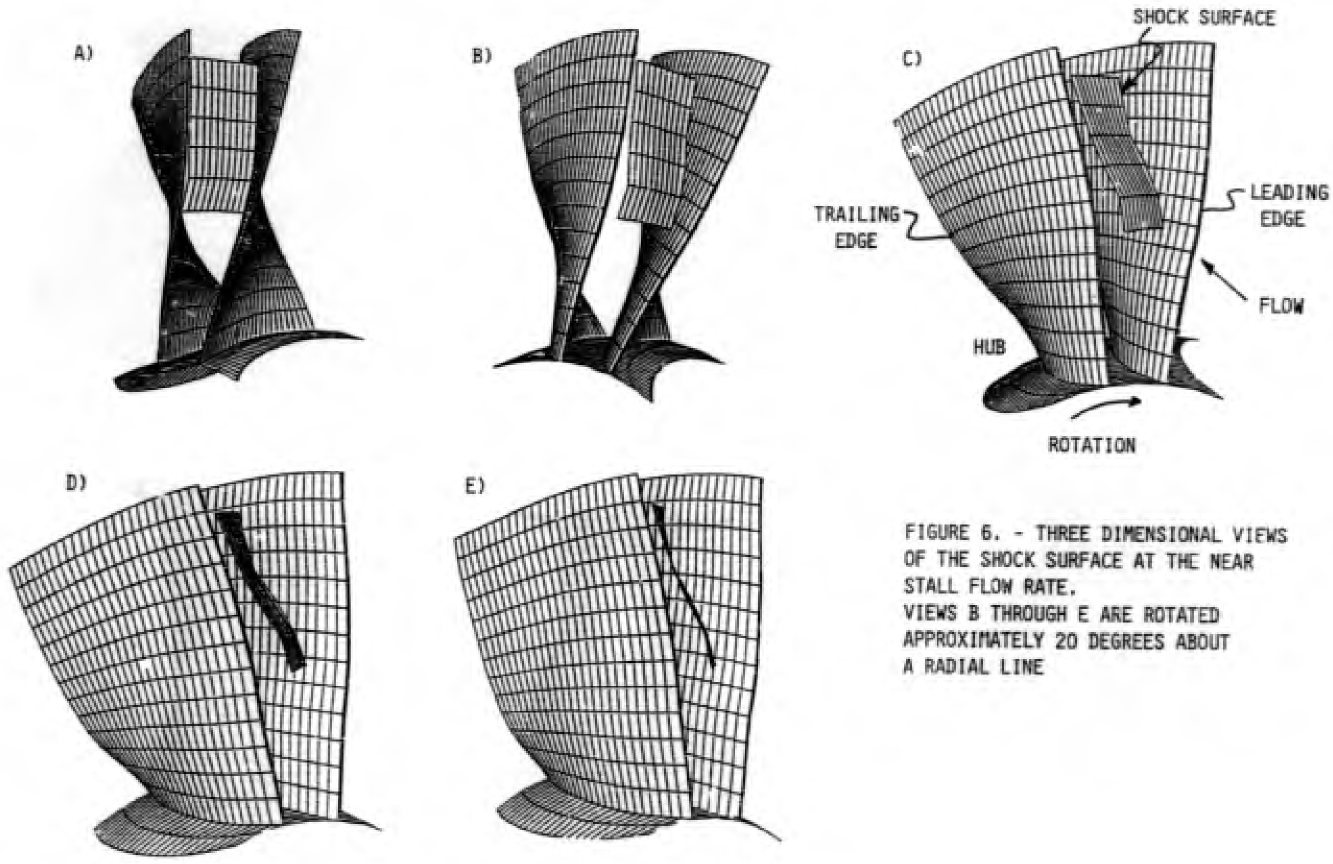

FIGURE 6. - THREE DIMENSIONAL VIEWS OF THE SHOCK SURFACE AT THE NEAR STALL FLOW RATE.
VIEWS B THROUGH E ARE ROTATED APPROXIMATELY 20 DEGREES ABOUT A RADIAL LINE

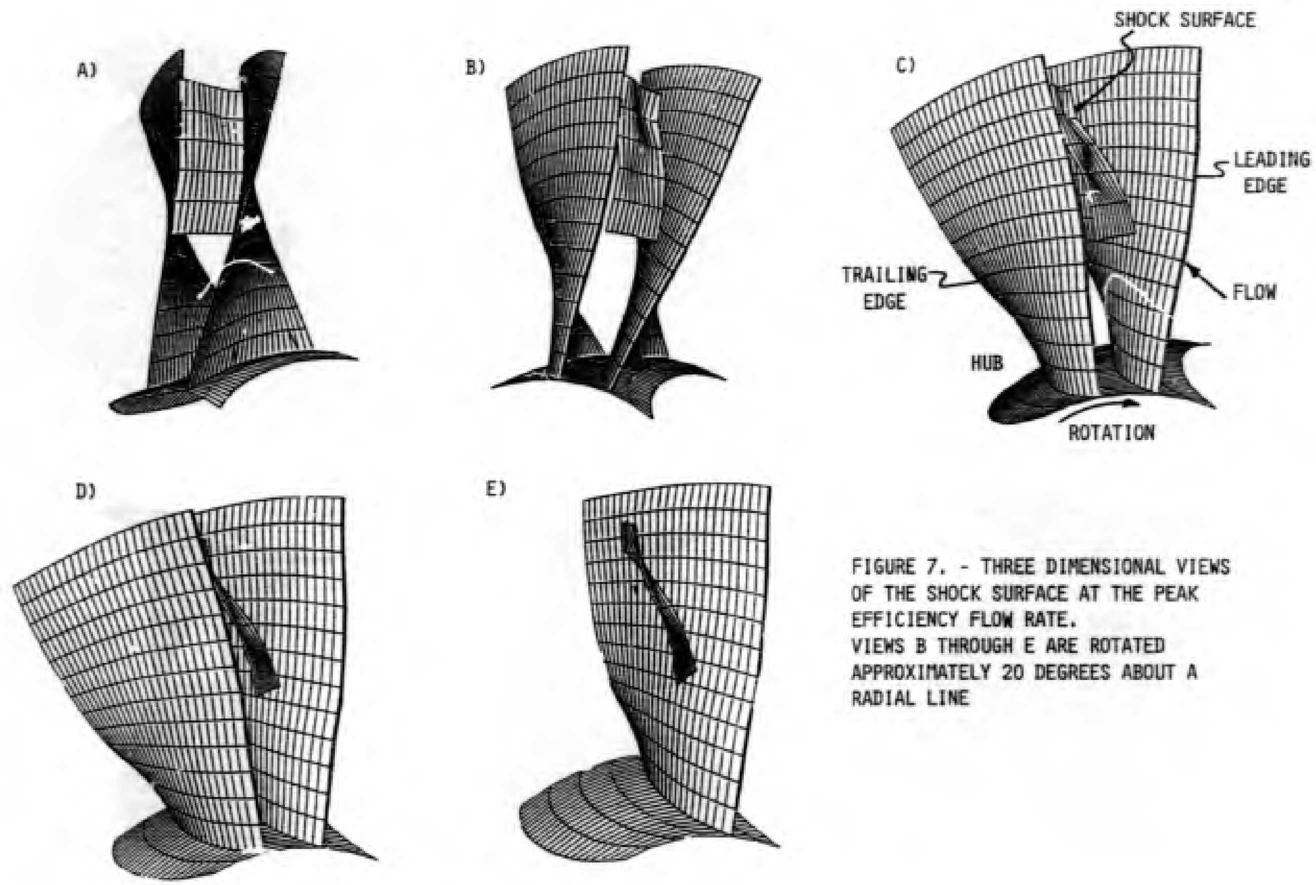

FIGURE 7. - THREE DIMENSIONAL VIEWS OF THE SHOCK SURFACE AT THE PEAK EFFICIENCY FLOW RATE.
VIEWS B THROUGH E ARE ROTATED APPROXIMATELY 20 DEGREES ABOUT A RADIAL LINE

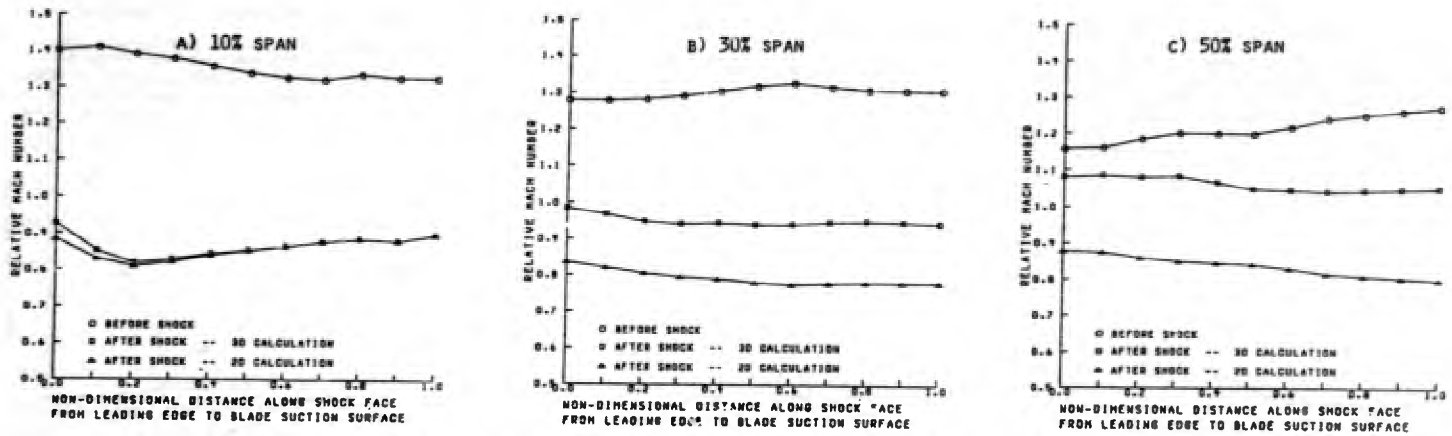

FIGURE 8. - RELATIVE MACH NUMBERS MEASURED BEFORE THE SHOCK AND CALCULATED AFTER THE SHOCK FOR NEAR STALL FLOW.

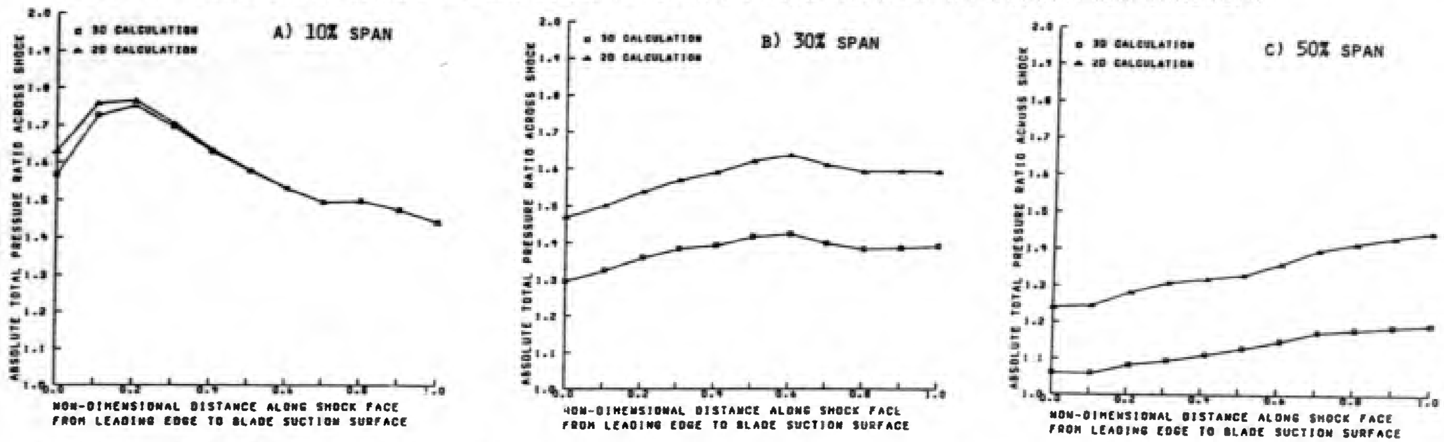

FIGURE 9. - TOTAL PRESSURE RATIO IN THE ABSOLUTE REFERENCE FRAME CALCULATED ACROSS THE SHOCK FOR NEAR STALL FLOW.

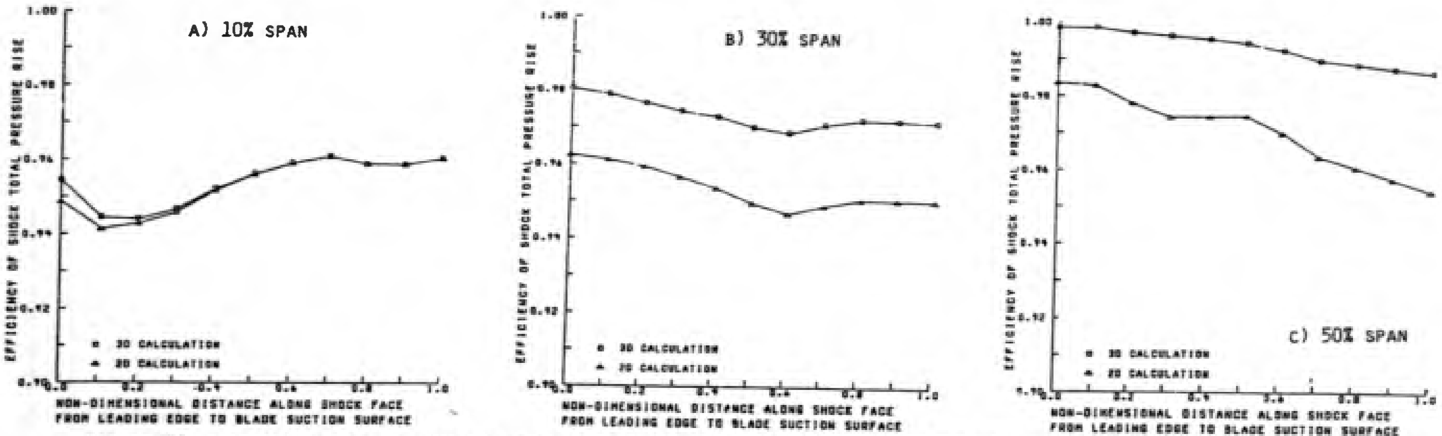

FIGURE 10. - EFFICIENCY OF THE TOTAL PRESSURE RISE CALCULATED ACROSS THE SHOCK FOR NEAR STALL FLOW.

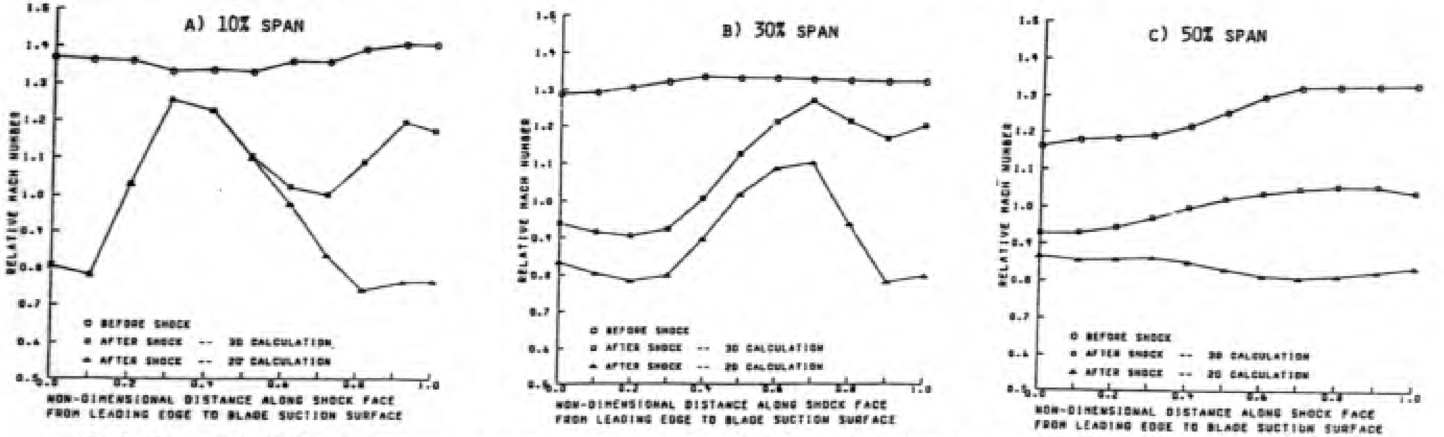

FIGURE 11. - RELATIVE MACH NUMBERS MEASURED BEFORE THE SHOCK AND CALCULATED AFTER THE SHOCK FOR PEAK EFFICIENCY FLOWS.

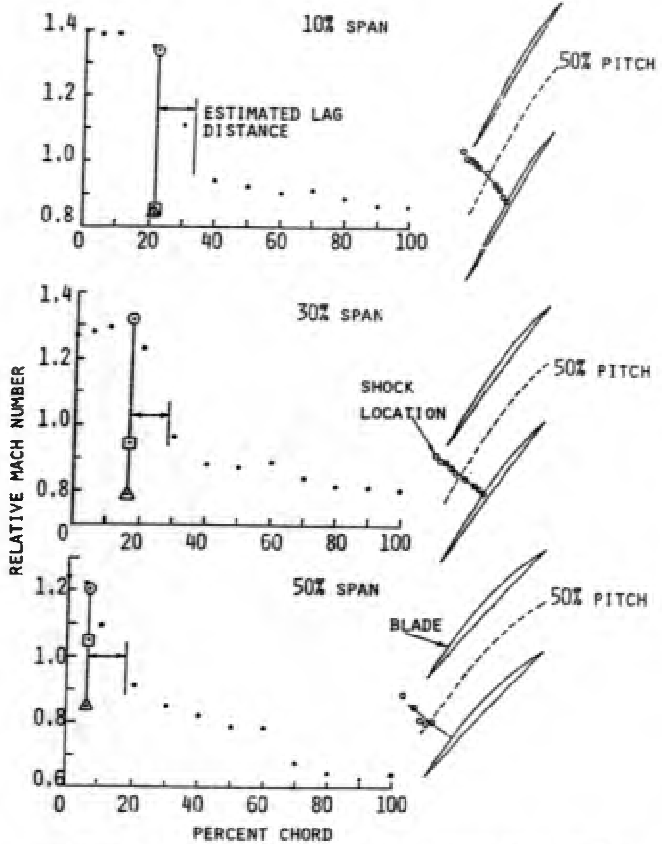

FIGURE 12A. - CHORDWISE PLOTS OF RELATIVE MACH NUMBER AT 50% PITCH FOR THE NEAR STALL FLOW RATE AT 10%, 30%, AND 50% SPAN.
● - DATA; ⊙ -BEFORE SHOCK; ⊡ -AFTER SHOCK --3D CALCULATION
△ -AFTER SHOCK -- 2D CALCULATION

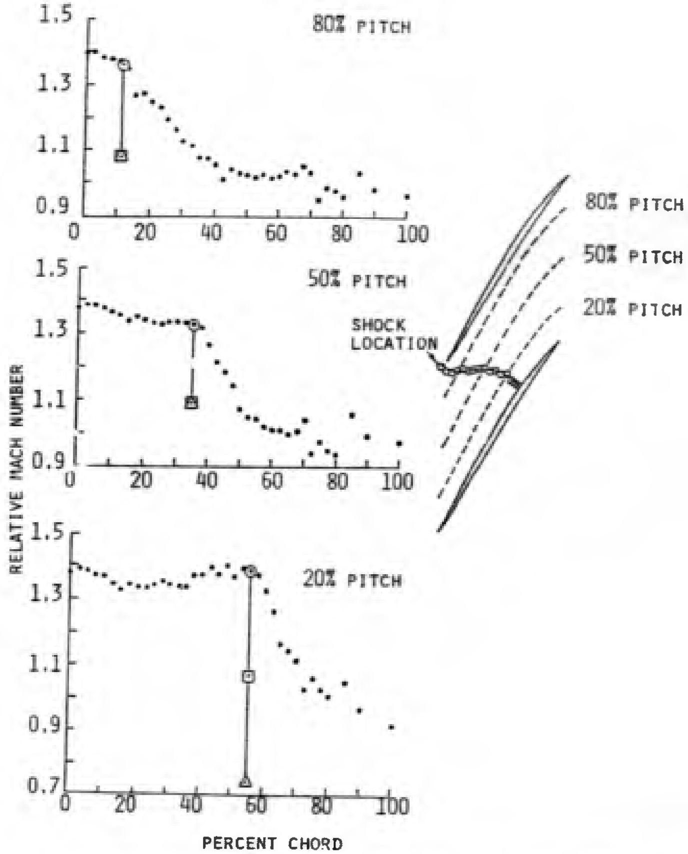

FIGURE 12B. - CHORDWISE PLOTS OF RELATIVE MACH NUMBER AT 10% SPAN FOR THE PEAK EFFICIENCY FLOW RATE AT 20%, 50%, AND 80% PITCH FROM THE SUCTION SURFACE.
●-DATA: ⊙-BEFORE SHOCK; ⊡ -AFTER SHOCK - 3D CALCULATION;
△ -AFTER SHOCK --2D CALCULATION

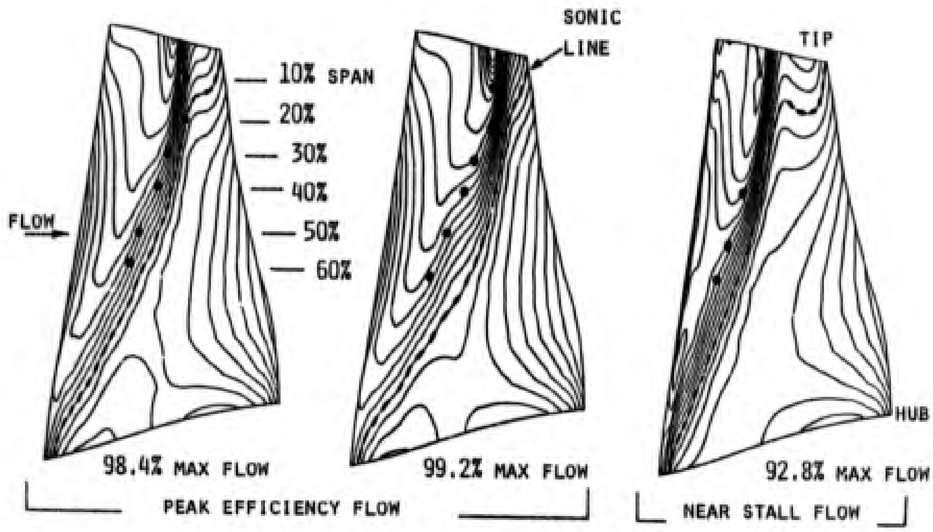

● - EXPERIMENTAL SHOCK LOCATIONS
PEAK EFFICIENCY FLOW RATE - 98.9% MAX FLOW
NEAR STALL FLOW RATE - 92.6% MAX FLOW

FIGURE 13. - COMPARISON OF SHOCK LOCATIONS ON THE BLADE SUCTION SURFACE FOR PEAK EFFICIENCY AND NEAR STALL FLOW RATES WITH ISOMACH LINES FROM A 3D EULER CALCULATION.

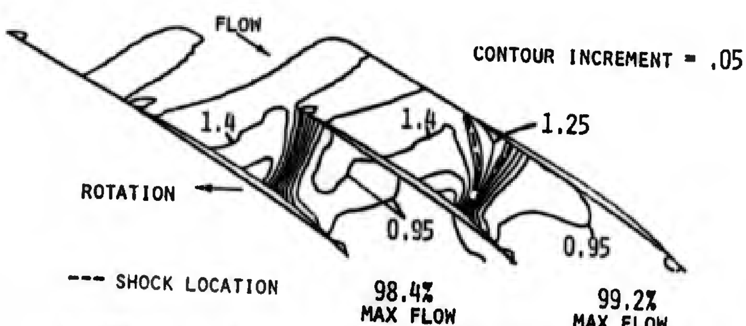

FIGURE 14. - ISOMACH LINES FROM A 3D EULER CALCULATION SHOWING TRANSITION FROM AN OBLIQUE SHOCK/PASSAGE SHOCK AT 99.2% MAXIMUM FLOW TO A SINGLE SHOCK AT 98.4% MAXIMUM FLOW AT 10% SPAN.

DISCUSSION

J.Fabri, Fr

Comment: From tests performed at ONERA by visualisation of flow fields in transonic or supersonic compressors, it appears that the leading edge shock wave is absolutely steady until near stall conditions. The downstream shock wave may be fluctuating at open throttle conditions.